PAPER

$Ba_9V_3Se_{15}$: a novel compound with spin chains

IOP Publishing Journal of Physics: Condensed Matter
J. Phys.: Condens. Matter **30** (2018) 214001 (9pp) https://doi.org/10.1088/1361-648X/aabdff

$Ba_9V_3Se_{15}$: a novel compound with spin chains

Jun Zhang[1,3], Min Liu[1,3], Xiancheng Wang[1], Kan Zhao[1], Lei Duan[1,3], Wenmin Li[1,3], Jianfa Zhao[1,3], Lipeng Cao[1], Guangyang Dai[1,3], Zheng Deng[1], Shaomin Feng[1], Sijia Zhang[1], Qingqing Liu[1], Yi-feng Yang[1,2,3] and Changqing Jin[1,2,3]

[1] Beijing National Laboratory for Condensed Matter Physics, Institute of Physics, Chinese Academy of Sciences, Beijing 100190, People's Republic of China
[2] Collaborative Innovation Center of Quantum Matter, Beijing 100190, People's Republic of China
[3] School of Physical Sciences, University of Chinese Academy of Sciences, Beijing 100190, People's Republic of China

E-mail: wangxiancheng@iphy.ac.cn, yifeng@iphy.ac.cn and jin@iphy.ac.cn

Received 20 December 2017, revised 27 March 2018
Accepted for publication 13 April 2018
Published 30 April 2018

Abstract

In this work, a novel compound $Ba_9V_3Se_{15}$ with one-dimensional (1D) spin chains was synthesized under high-pressure and high-temperature conditions. It was systematically characterized via structural, magnetic, thermodynamic and transport measurements. $Ba_9V_3Se_{15}$ crystallizes into a hexagonal structure with a space group of P-6c2 (188) and the lattice constants of $a = b = 9.5745(7)$ Å and $c = 18.7814(4)$ Å. The crystal structure consists of face-sharing octahedral VSe_6 chains along c axis, which are trimeric and arranged in a triangular lattice in ab-plane. $Ba_9V_3Se_{15}$ is a semiconductor and undergoes complex magnetic transitions. In the zero-field-cooled (ZFC) process with magnetic field of 10 Oe, $Ba_9V_3Se_{15}$ sequentially undergoes ferrimagnetic and spin cluster glass transition at 2.5 K and 3.3 K, respectively. When the magnetic field exceeds 50 Oe, only the ferrimagnetic transition can be observed. Above the transition temperature, the specific heat contains a significant magnetic contribution that is proportional to $T^{1/2}$. The calculation suggests that the nearest neighbor (NN) intra-chain antiferromagnetic exchange J_1 is much larger than the next nearest neighbor (NNN) intra-chain ferromagnetic exchange J_2. Therefore, $Ba_9V_3Se_{15}$ can be regarded as an effective ferromagnetic chains with effective spin-1/2 by the formation of the $V(2)^{(\downarrow)}V(1)^{(\uparrow)}V(2)^{(\downarrow)}$ cluster.

Keywords: one dimension, spin chain, ferromagnetic chains, specific heat

(Some figures may appear in colour only in the online journal)

Introduction

$BaVS_3$ has received a lot of attention because of its rich physical phenomena [1–9], such as metal-insulator (MI) transition driven by Peierls instability [5]. $BaVS_3$ is a spin-1/2 chain system where the crystal structure consists of face-sharing octahedral VS_6 chains. At room temperature $BaVS_3$ crystalizes into hexagonal structure ($P63/mmc$) with VS_6 chains packed in a triangular lattice in ab-plane. The intra-chain nearest V–V distance is 2.807 Å, much smaller than that of inter-chain (6.713 Å), thereby, presenting a quasi 1D structure. It undergoes a sequence of phase transitions: structural phase transition to $Cmc21$ space group at 240 K due to the zigzag deformation of VS_6 chains [10], MI transition with $T_{MI} \sim 69$ K accompanied by another structural phase transition to Im space group [5] and incommensurate antiferromagnetic order (ICAFO) transition at $T_N \sim 31$ K [7]. Far beyond T_{MI}, 1D lattice fluctuations have been revealed, which is responsible for the tetramerization of the VS_6 chains and the formation of charge density order, further leading to the MI transition. Between T_{MI} and T_N, although the long range magnetic order has not emerged, the presence of long-range and dynamic

antiferromagnetic correlation has been evidenced, which is analogous with a spin-liquid state [3]. Corresponding to the ICAFO transition, there is no anomaly in the specific heat measurement [2]. In the ICAFO state, the spins are oriented along *a* axis in the monoclinic structure. The ordering is antiferromagnetic in *ab*-plane and predominantly ferromagnetic with long range modulation along *c* axis [7].

Applying high pressure to $BaVS_3$ can gradually suppress the MI transition and induce quantum critical point at ~2GPa [9]. Chemical pressure introduced by Sr-doping also can suppress the MI and ICAFO transition, after which a ferromagnetic order appears when Sr-doping level exceeds 0.1 [11]. As an isostructural counterpart of $BaVS_3$, $BaVSe_3$ exhibits similar structural transition from hexagonal to orthorhombic phase at 310 K [12]. However, the important difference is that $BaVSe_3$ is a ferromagnetic metal with *c* easy axis and $T_C \sim 43$ K, which behaves like $BaVS_3$ under chemical pressure [13, 14]. Just above T_C, $BaVSe_3$ is revealed to undergo a magnetic symmetry change at 62.5 K from the anisotropy of $\chi_c < \chi_\perp$ to $\chi_c > \chi_\perp$ [15]. In the paramagnetic state, the magnetic susceptibility follows the Curie–Weiss form, and the Curie–Weiss temperature ($T_\theta \sim 44$ K) is very close to T_C (43 K), which demonstrates less magnetic frustration in $BaVSe_3$. Compared with $BaVS_3$, $BaVSe_3$ presents less physical properties associated with spin chains.

How about increasing the distance of adjacent inter-chains in the vanadium chalcogenides? Learning from the 1D structure of $Ba_9Fe_3S_{15}$ [16] and $Ba_9Sn_3Te_{15}$ [17], we substitute the cation of Fe/Sn with V as well as the anion of S/Te with Se, and successfully synthesize the new compound $Ba_9V_3Se_{15}$ under high-pressure and high-temperature conditions. It crystalizes into a hexagonal structure with a space group *P*-6*c*2 (188). Similar to $BaVS_3$ and $BaVSe_3$, the structure of $Ba_9V_3Se_{15}$ consists of face-sharing VSe_6 chains that are packed in a triangular lattice in *ab*-plane. However, the distance of adjacent chains (9.5745(7) Å) in $Ba_9V_3Se_{15}$ is much larger than $BaVS_3$ and $BaVSe_3$, demonstrating that $Ba_9V_3Se_{15}$ further approaches to one dimensionality in the view of crystal structure. $Ba_9V_3Se_{15}$ undergoes a ferrimagnetic transition at 2.5 K. At low temperature, there is a significant magnetic specific heat, which is proportional to $T^{1/2}$. $Ba_9V_3Se_{15}$ can be regarded as an effective ferromagnetic chains with effective spin-1/2 by the formation of the $V(2)^{(\downarrow)}V(1)^{(\uparrow)}V(2)^{(\downarrow)}$ cluster.

Experimental and calculations

A polycrystalline sample of $Ba_9V_3Se_{15}$ was synthesized under the conditions of high-pressure and high-temperature. The commercially available crystalline powders of V (Alfa, >99.5% pure), Se (Alfa, >99.999% pure) and lumps of Ba (Alfa, immersed in oil, >99.2% pure) were used as the starting materials. The precursor BaSe was prepared by heating the mixture of Ba blocks and Se powder in an alumina crucible sealed in an evacuated quartz tube at 700 °C for 20 h. The mixture of BaSe, V and Se were homogenously mixed according to a molar ratio 3:1:2 and was pressed into a pellet with a diameter of 6 mm. The pre-pressed pellet was placed in an h-BN capsule and then put into a furnace of graphite tube. High pressure experiments were performed in a DS6 × 600 T cubic anvil high pressure apparatus. After pressure was slowly raised to 5.5 GPa, the sample was heated to 1400 °C within 4 min and kept for 40 min. After the high-pressure and high-temperature process, the black pure polycrystalline sample of $Ba_9V_3Se_{15}$ was obtained.

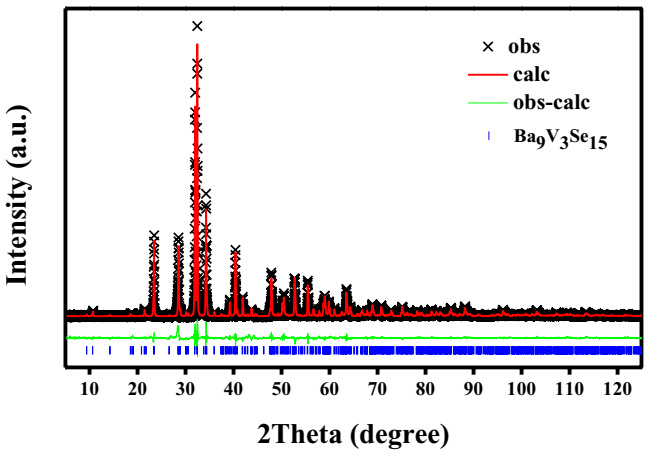

Figure 1. X-ray powder patterns of $Ba_9V_3Se_{15}$ measured at room temperature and the refinement with the space group of *P*-6*c*2 (188).

The powder x-ray diffraction was performed on a Rigaku Ultima VI (3KW) diffractometer using Cu Kα radiation generated at 40 kV and 40 mA. The data was collected at a scanning rate of 1° per min with a scanning step length of 0.02°. The Rietveld refinement on the diffraction spectra was carried out by using Gsas software packages. The dc magnetic susceptibility was measured using a superconducting quantum interference device (SQUID). The electronic conductivity, *ac* susceptibility and specific heat were measured using a physical property measuring system (PPMS).

The electronic structures were obtained by density functional theory (DFT) calculations using the full-potential linearized augmented plane-wave (LAPW) method [18], with the augmented plane-wave plus local orbitals implementation [19] both in the WIEN2k code [20]. To include the strong correlations in the transition-metal elements, we took the generalized gradient approximation-Perdew, Burke and Ernzerhof (GGA-PBE) exchange correlation potential [21] with an effective Coulomb repulsion $U^{\text{eff}} = 5$ eV for V in the GGA + *U* calculations [22]. The Muffin-tin radii R_{MT} are 2.50 a.u. for Ba, 2.50 a.u. for V, and 2.40 a.u. for Se, respectively. The maximum modulus for the reciprocal vectors K_{max} was chosen such that $R_{\text{MT}} * K_{\text{max}} = 8.0$ and 1000 k-points meshes were used in the whole Brillouin zone.

Results and discussions

Figure 1 shows the powder x-ray diffraction patterns of $Ba_9V_3Se_{15}$ sample. All the peaks can be indexed in a hexagonal structure with the lattice parameters of $a = b = 9.5745(7)$ Å and $c = 18.7814(4)$ Å. The systematic absence of *hkl* suggests that the space group should be *P*-6*c*2 (188). Here, the structures of $Ba_9Fe_3S_{15}$ and newly discovered compounds $Ba_9Sn_3Te_{15}$ reported in our previous work were adopted to refine the diffraction data of the $Ba_9V_3Se_{15}$ [16, 17]. Using

Table 1. The summary of the crystallographic data at room temperature for $Ba_9V_3Se_{15}$.

Compound			$Ba_9V_3Se_{15}$				
Space group: *P*-6 *c* 2 (188)—hexagonal $a = b = 9.5745$ (7) (Å), $c = 18.7814$ (4) (Å) $V = 1491.07$ (0) (Å^3), $Z = 2$ $\chi^2 = 2.8$, wRp = 5.6%, Rp = 4.2%							
Atom	Label	Wyck.	*x*/*a*	*y*/*b*	*z*/*c*	SOF	*U* (Å^2)
Ba	Ba1	12l	0.0144(7)	0.3825(7)	0.0859(4)	1	0.021
Ba	Ba2	6k	0.3956(4)	0.3776(8)	0.25000	1	0.023
V	V1	2a	0	0	0	1	0.022
V	V2	4g	0	0	0.1685(3)	1	0.014
Se	Se1	12l	0.2275(8)	0.2208(8)	0.0871(5)	1	0.025
Se	Se2	6k	0.0126(2)	0.2336(1)	0.25000	1	0.031
Se	Se3	2c	1/3	2/3	0	1	0.032
Se	Se4	4h	1/3	2/3	0.1859(8)	1	0.019
Se	Se5	4i	2/3	1/3	0.1658(8)	1	0.004
Se	Se6	4i	2/3	1/3	0.0505(6)	0.5	0.023

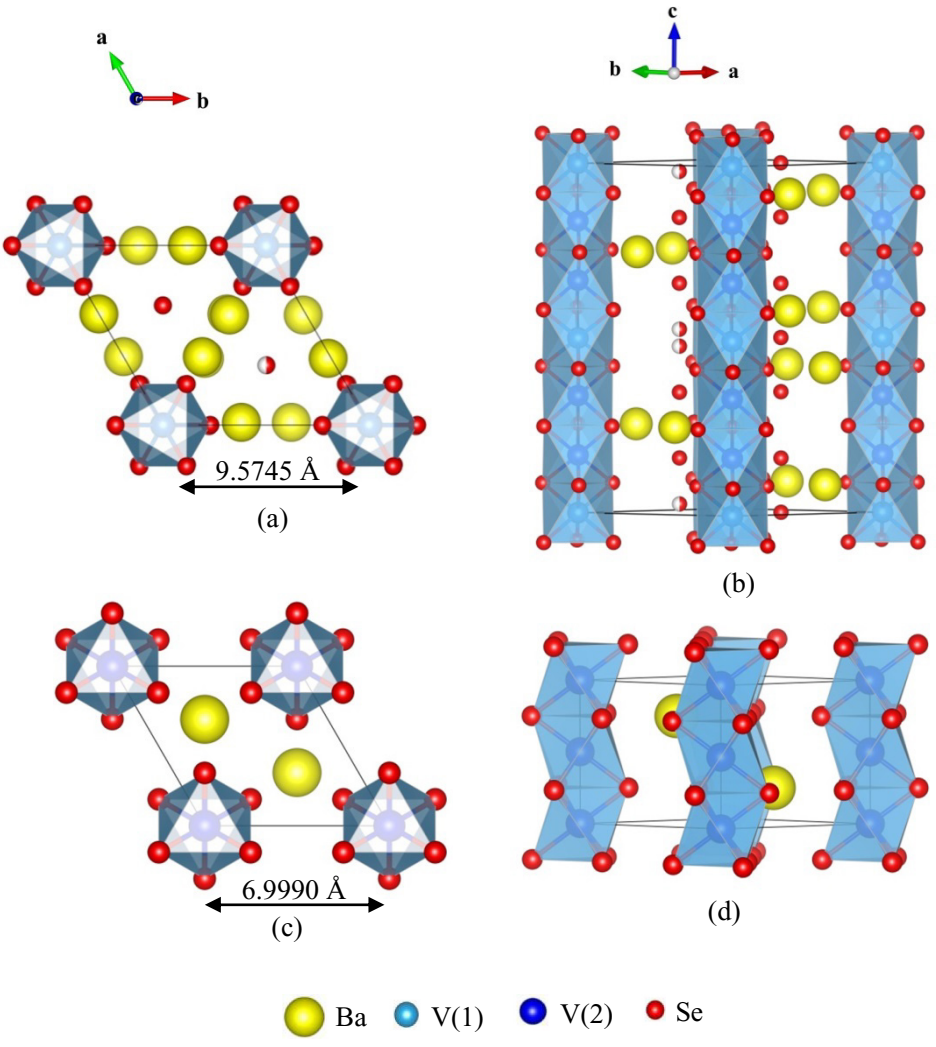

Figure 2. The crystal structures of $Ba_9V_3Se_{15}$ and $BaVSe_3$, showing the face-sharing octahedron VSe_6 chains. (a) and (c) is the top view with the projection along *c* axis for $Ba_9V_3Se_{15}$ and $BaVSe_3$, respectively; (b) and (d) is the perspective view with the projection along [1 1 0] direction.

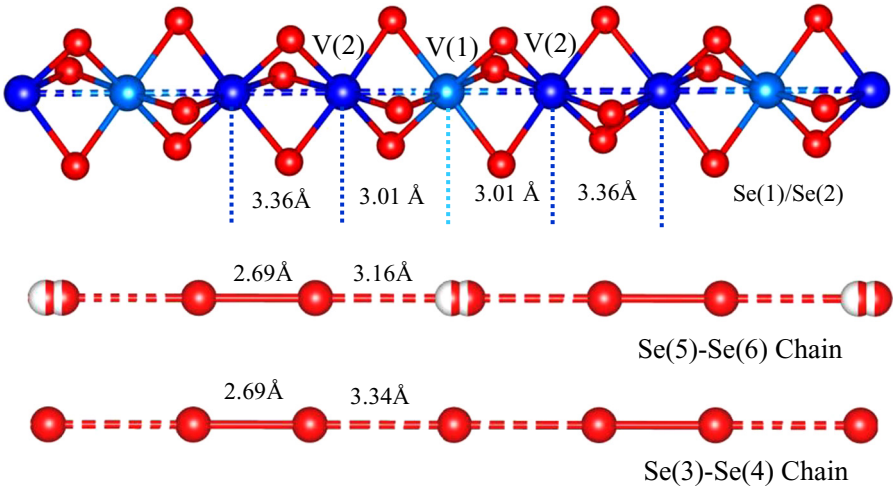

Figure 3. The sketch of VSe_6 octahedral chains and Se chains in the compound of $Ba_9V_3Se_{15}$.

GSAS software packages the refinements were conducted and smoothly converged to $\chi^2 = 2.8$, Rp = 4.2% and Rwp = 5.6% for $Ba_9V_3Se_{15}$. The summary of the crystallographic data at room temperature is shown in table 1.

Based on the refinement results, the crystal structure of $Ba_9V_3Se_{15}$ is sketched in figures 2(a) and (b). For comparison, the structure of $BaVSe_3$ is also shown in figures 2(c) and (d). Both crystal structures of $Ba_9V_3Se_{15}$ and $BaVSe_3$ contain face-sharing octahedral VSe_6 chains along *c* axis, which are arranged in a triangular lattice in *ab*-plane. As for the VSe_6 chains, there are three remarkable differences between the two compounds. One is the distance of the adjacent chains, which is given by their lattice constant *a*, shown in figures 2(a) and (c) respectively. For $Ba_9V_3Se_{15}$, the VSe_6 chains are separated by two octahedral $SeBa_6$ chains. Thus, the distance of adjacent chains is significantly enlarged from 6.9990 Å ($BaVSe_3$) to 9.5745 Å, and $Ba_9V_3Se_{15}$ presents further approaching to one dimensionality. The second is that the distance of adjacent V atoms within the chains in $BaVSe_3$ are equal (2.93 Å); while the VSe_6 chains in $Ba_9V_3Se_{15}$ are trimeric, leading to two sites for V atoms. In a trimeric unit, there are one *V*(1) atom and two *V*(2) atoms. The distances of adjacent V atoms are 3.01 Å and 3.36 Å, shown in figure 3. The third is the oxidation state of V. For $BaVSe_3$, the valence of V is +4, so that the 3d orbital is occupied with only one electron. Therefore, $BaVSe_3$ is considered to be the system with spin-1/2 chains. However, it is a little complex in $Ba_9V_3Se_{15}$. Assuming the valence of all the Se anions in $Ba_9V_3Se_{15}$ is −2, the oxidation state of V should be +4 to balance the charge to be neutral. However, this is not the case. Figure 3 also shows the sketch of Se chains composed of Se(3)-Se(4) and Se(5)-Se(6) atoms in $Ba_9V_3Se_{15}$. The distances between the adjacent Se in the chains are 2.69 Å, 3.16 Å and 3.34 Å, respectively. In polyselenides, such as Ba_2SnSe_5 and Sr_2SnSe_5, the Se atoms can form bonds with the bond length ranging from 2.38 Å to 2.44 Å as well as the typical bond angle from106° to 111° [23, 24]. In the Se chains of $Ba_9V_3Se_{15}$, the distance of 2.69 Å is very close to that of bonded Se atoms, suggesting the formation of Se_2^{2-} dimer. The similar Te_2^{2-} (Se_2^{2-}) dimer has also been reported in $Ba_9Sn_3Te_{15}$ ($Ba_9Sn_3Se_{15}$) [17]. Following the calculated results of the oxidation state of +2 for *V*(1) and +3 for *V*(2) (see the calculations below) and based on the site symmetry and the charge balance, the molecular formula of $Ba_9V_3Se_{15}$ can be rewritten as $Ba^{2+}{}_9V^{2+}V^{3+}{}_2Se_9^{2-}\left(Se^{1-}{}_4Se_2^{2-}\right)$.

Figure 4(a) shows the temperature dependence of resistivity of $Ba_9V_3Se_{15}$. The resistivity at room temperature is about 24 $\Omega \cdot$ mm. The resistivity increases with decreasing temperature, thereby demonstrating a semiconducting behavior. The inset is the curve of lnρ versus inverse temperature, presenting a straight line. By using the formula of $\rho \propto \exp(\Delta_g/2k_BT)$, where Δ_g is the semiconducting band gap and k_B is the Boltzmann's constant, the resistivity curve can be well fitted and the band gap Δ_g is evaluated to be 0.2 eV. Figures 4(b) and (c) shows the temperature dependence of magnetic susceptibility measured with $H = 1000$ Oe and the magnetic hysteresis curve, respectively. The $M(H)$ curve is linear at 10 K and 20 K. When the temperature is cooled down to 5 K, the magnetization $M(H)$ exhibits a negative curvature. At 1.8 K, the saturated magnetic moment is close to 1 μ_B/f.u. Figure 4(b) also displays the curve of inverse susceptibility as a function of temperature. By using the Curie–Weiss law $1/\chi = T/C - T_\theta/C$, linearly fitting the curve of high temperature region gives the effective magnetic moment $\mu_{eff} \sim 5.3$ μ_B/f.u. and the Curie–Weiss temperature $T_\theta \sim 31$ K. Given the molecular formula $Ba^{2+}{}_9V^{2+}V^{3+}{}_2Se_9^{2-}\left(Se^{1-}{}_4Se_2^{2-}\right)$, there are three electrons in the 3*d* orbital for *V*(1) atoms and two electrons for *V*(2). In addition, the bellowing calculations suggest an antiferromagnetic NN intra-chain interaction, which results in a cluster of $V(2)^{(\downarrow)}V(1)^{(\uparrow)}V(2)^{(\downarrow)}$. Therefore, the theoretical value of the effective moment is $g\mu_B\sqrt{\frac{3}{2}\times\left(\frac{3}{2}+1\right)+2\times\frac{2}{2}\times\left(\frac{2}{2}+1\right)} \approx 5.7\mu_B$/f.u. and the saturated moment μ_{sat} is 1 μ_B/f.u., where the Lande factor *g* is assigned to be 2. Thus, the values of μ_{eff} and μ_{sat} deduced from the magnetic measurements agree with the calculations. As will be discussed later, the spin chains are effectively decoupled in the experimental temperature range above the magnetic transition, and can be regarded as an effective ferromagnetic chains with effective spin-1/2

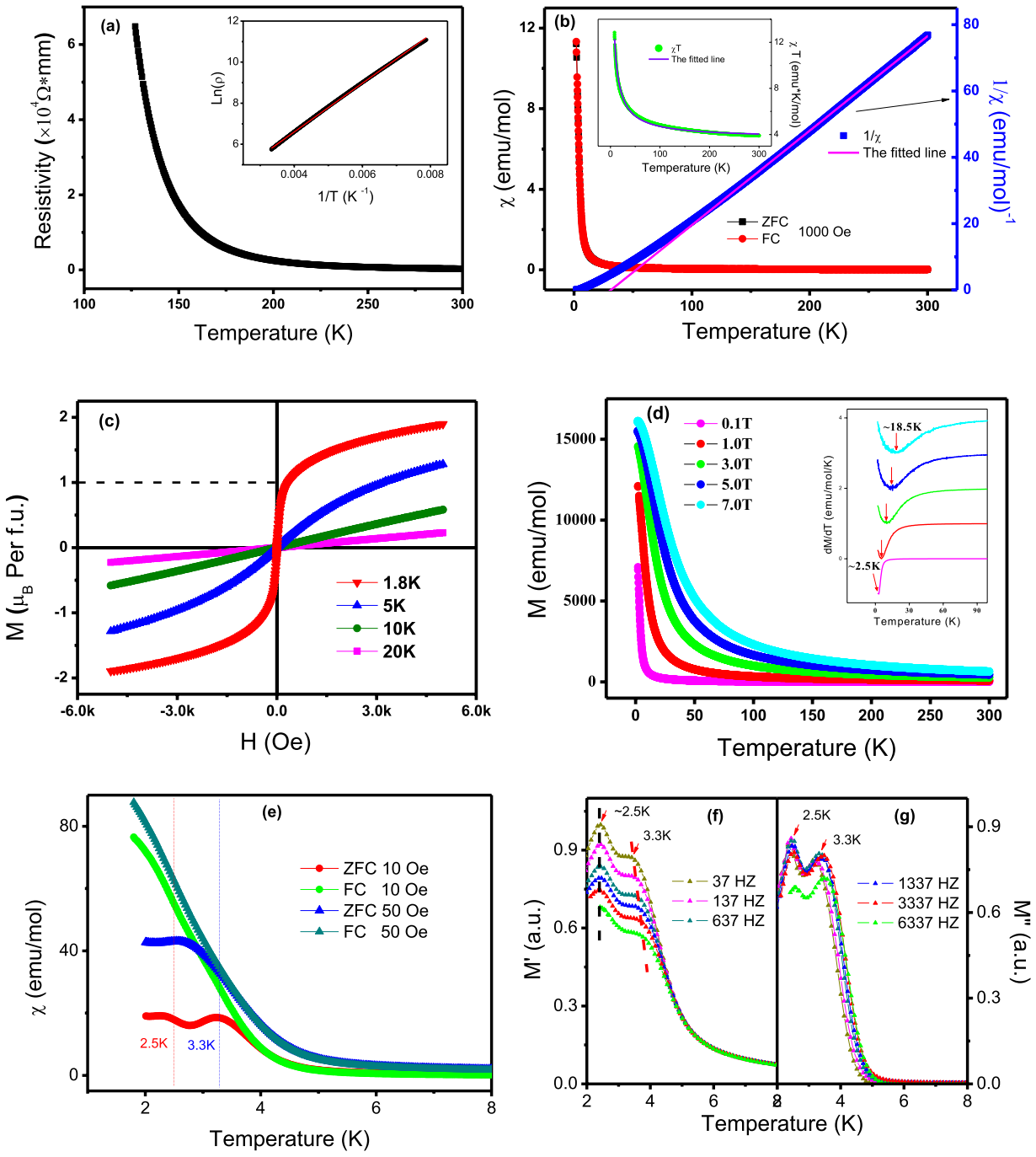

Figure 4. (a) The resistivity as a function of temperature, and the inset shows the ln (ρ) versus inverse temperature. (b) The temperature dependence of susceptibility χ measured with $H = 1000$ Oe and the inverse susceptibility $1/\chi$ versus T. The inset is the temperature dependence of χT and the fitting curve. (c) The magnetic hysteresis curves measured at different temperatures. (d) The temperature dependence of magnetization measured under different magnetic fields. The inset is the temperature derivative of magnetization dM/dT. (e) The susceptibility χ measured with $H = 10$ and 50 Oe. (f) and (g) The *ac* magnetic susceptibility measured at different frequencies.

by the formation of the $V(2)^{(\downarrow)}V(1)^{(\uparrow)}V(2)^{(\downarrow)}$ cluster. Thus, a better fit for the measured susceptibility may be obtained using the following approximate scaling formula for the ferromagnetic spin-1/2 Heisenberg model [25]:

$$\chi T = C\left[1 + 0.6J(S+1)\frac{1}{T}\right]^{1.25S}$$

where $S = 1/2$ is the spin moment and $J = J_2$ is the inter-cluster interaction. This is indeed the case, as shown in the inset of figure 4(b). The deduced value of J is about 53 K, consistent with the Curie–Weiss temperature of 31 K and the estimated value of $J_2 \sim 47$ K derived from our first-principles numerical calculations (see below).

Figure 4(d) displays the temperature dependence of magnetization measured under different magnetic fields. When the field is 7T, the magnetization curve exhibits saturation at low temperature. The inset of figure 4(d) is the temperature derivative of magnetization dM/dT, from which the ferrimagnetic

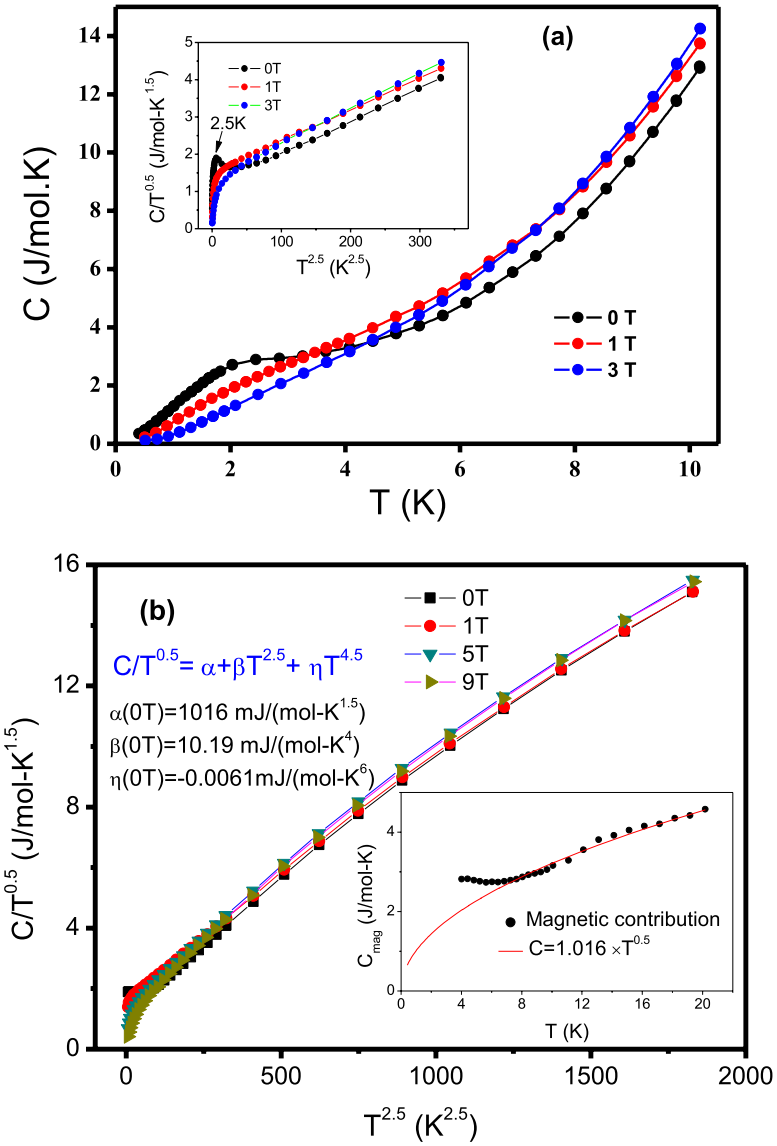

Figure 5. (a) Specific heat data with the temperature down to 0.4 K for $Ba_9V_3Se_{15}$; the inset shows the $C/T^{1/2}$ as a function of $T^{2.5}$ for $Ba_9V_3Se_{15}$. (b) Specific heat measurement for another sample of $Ba_9V_3Se_{15}$ in a wide temperature region. The inset is the specific heat subtracted by the lattice contribution, and the fitted line of $T^{0.5}$ dependence of SH is shown with the red line.

transition temperature can be determined. It can be seen from the inset that the ferrimagnetic transition temperature increases with magnetic field increases, which is a general phenomenon for a ferromagnetic system. Figure 4(e) shows the magnetic susceptibility measured with the magnetic field of 10 Oe and 50 Oe, respectively, where the ZFC curves and FC curves divaricate below 4 K. When the field is 10 Oe, the ZFC curve presents two kinks, corresponding to the ferrimagnetic transition at 2.5 K and spin cluster glass frozen temperature at 3.3 K, respectively. For the field of 50 Oe, the formation process of spin cluster glass cannot be observed and the separation of ZFC and FC curves implies the existence of magnetic hysteresis. The two phase transitions at low field can be further confirmed by the *ac* magnetic susceptibility measurement, which is presented in figures 4(f) and (g). Both the real and imaginary parts exhibit two maximums at 2.5 K and ~3.3 K, respectively. The maximum at 2.5 K is independent on frequency; while the other one shifts towards higher temperature when frequency increases, demonstrating spin cluster glass behavior.

For an ideal 1D spin chain, no long-range magnetic order can exist at finite temperature as implied in the Mermin–Wagner theorem [26]. On the other hand, the inter-chain coupling between spin chains may govern the magnetic order although it is in general much weaker than intra-chain couplings [27]. In addition, if the 1D spin chains are arranged in a triangular lattice, there also exists magnetic frustration due to the special geometric structure of triangular arrangement and antiferromagnetic inter-chain interaction. A prominent example is ABX_3 system where A is alkali metal, B is transition metal and X is a halogen atom [28]. In these materials, there are chains containing atom B (normally magnetic) along the *c* axis, and the distance of adjacent chains is typically about 7.5 Å. Most of these compounds are antiferromagnetic with a rich magnetic phase diagram due to the magnetic frustration, and the magnetic structure can be tuned by magnetic field. While for $Ba_9V_3Se_{15}$, the distance of adjacent chains is much larger than ABX_3 system, hinting an even weaker inter-chain interaction. The spin cluster glass state should arise

from the spin frustration. A small magnetic field can eliminate the spin cluster glass state and orientates the spin to the magnetic direction. Here, we cannot tell the detailed magnetic structure, which deserves to be further studied by neutron diffraction measurement.

Figure 5 shows the temperature dependence of specific heat (SH) for two samples of $Ba_9V_3Se_{15}$. Figure 5(a) is the data measured in the temperature range from 0.4 K to 10 K. As shown in the figure 5(a), there is a broad maximum centered at about 2.5 K. Although the broad maximum can be usually expected in an ideal spin chain system [29–31], the broad SH peak is also a common phenomenon in quasi 1D spin-chain compounds, due to the development of short-range ordering along the chains before 3D magnetic ordering formation [32, 33]. With the applied magnetic field increasing, the SH peak shifts to higher temperature and becomes broader and nearly disappears at 3T. At the same time, the SH curve upshifts, hinting the weight of magnetic contribution moves to higher temperature. The behavior of magnetic SH responding to the applied magnetic field is consistent with that for a ferro- or ferri- magnetic system. As suggested by the following calculations that the NN intra-chain antiferromagnetic exchange J_1 is two orders of magnitude larger than NNN intra-chain ferromagnetic exchange J_2, the chains in $Ba_9V_3Se_{15}$, therefore, can be regarded as an effective ferromagnetic chains with effective spin-1/2 by the formation of $V(2)^{(\downarrow)}V(1)^{(\uparrow)}V(2)^{(\downarrow)}$ cluster. It should be noted that, for $Ba_9V_3Se_{15}$, there are three energy scales of NN intra-chain exchange J_1, NNN intra-chain exchange J_2 and inter-chain exchange J_3, which governs the $V(2)^{(\downarrow)}V(1)^{(\uparrow)}V(2)^{(\downarrow)}$ cluster formation, the development of ferromagnetic short-range order in the chains and the 3D magnetic transition, respectively. Just above the 3D magnetic transition, the chains are decoupled and the magnetic SH should be dominant by the spin wave excitation arising from the spin chains. As predicted by the spin wave theory, ferromagnetic chains host a quadratic magnon excitation with $\omega \sim k^2$, which should lead to a $T^{1/2}$ magnetic SH at low temperature. Thus, we use the formula of $C = \alpha T^{1/2} + \beta T^3$ to analysize the low temperature SH data, where the first term is the magnetic contribution and the second term is the phonon contribution. The inset of figure 5(a) shows the curve of SH divided by square root temperature $C/T^{1/2}$ versus $T^{2.5}$. The magnetic transition temperature can be unambiguously determined by the peak at 2.5 K. Above the transition, the curve of $C/T^{1/2}$ versus $T^{2.5}$ is nearly linear in the low temperature region, which can be fitted using the formula of $C/T^{1/2} = \alpha + \beta T^{2.5}$, where α and β is the coefficient associated with magnetic and phonon SH, respectively. The value of α can be evaluated to be 1096–1458 mJ $(\text{mol} \cdot K^{1.5})^{-1}$ depending on magnetic field. To confirm the result, we carried out SH measurement on another sample in a wider temperature range from1.8 K to 20 K with the magnetic field up to 9T, which is shown in figure 5(b). The curve of $C/T^{1/2}$ versus $T^{2.5}$ is slightly deviated from a straight line. Here, the formula of $C/T^{1/2} = \alpha + \beta T^{2.5} + \eta T^{4.5}$, where η is the quintic term coefficient of the phonon SH, can be used to fit the SH data. The fitted parameters are shown in table 2. After subtracting the lattice contribution, the magnetic SH data of zero magnetic field is shown in the inset of figure 5(b). The data away from the 3D magnetic transition can be well fitted with a $T^{0.5}$-dependent line, which demonstrates the magnetic SH of the decoupled chains in $Ba_9V_3Se_{15}$ can be described by the spin wave theory.

Table 2. The parameters obtained by using the formula $C/T^{1/2} = \alpha + \beta T^{2.5} + \eta T^{4.5}$ to fit the specific heat data.

	α mJ $(\text{mol} \cdot \text{K}^{1.5})^{-1}$	β mJ $(\text{mol} \cdot \text{K}^{4})^{-1}$	η mJ $(\text{mol} \cdot \text{K}^{6})^{-1}$
0T	1016	10.19	−0.0061
1T	1416	9.67	−0.0053
5T	1214	10.67	−0.0007
9T	1042	10.88	−0.0074

The electronic and magnetic structures of $Ba_9V_3Se_{15}$ were further investigated by the first-principles calculations. To determine the magnetic ground state, GGA and GGA + U spin-polarized calculations were performed for different magnetic structures (see figure 6). Both yield a cluster ferrimagnetic $V(2)^{(\downarrow)}V(1)^{(\uparrow)}V(2)^{(\downarrow)}$ ground state, in good agreement with experimental analysis. Here, we have used $U_{\text{eff}} = 5$ eV for V in the GGA + U calculations, following the common choices in the literature [34]. Other values of U_{eff} in a wide range around the above choice have also been tested, and yield the same magnetic ground state. We obtain a total magnetic moment of 0.999 μ_B/f.u. with the atomic contributions of V_1 and V_2 inside the muffin-tin spheres to be 2.592 μ_B, and −1.998 μ_B, respectively. These indicate that the local spins on the V_1 and V_2-ions are approximately $S_1 = 3/2$ and $S_2 = 1$, respectively. The values of the ionic magnetic moments are slightly reduced from their ideal values because of the strong hybridization with Se-p orbitals.

The electronic density of states (DOS) and band structures of $Ba_9V_3Se_{15}$ from the GGA + U calculation are shown in figure 7. We find an insulating gap of 0.66 eV in the spin up channel and 0.58 eV in the spin down channel. These confirm the insulating nature of the electronic ground state. The obtained values are somewhat larger than that derived from experiments, which is, however, not unexpected as GGA + U calculations typically overestimate the insulating gap. Away from the Fermi energy, the bands show a larger dispersion along k_z direction (the A-Gamma path) and are flat within the *ab* plane (the Gamma-M path), manifesting the quasi 1D structure of $Ba_9V_3Se_{15}$. Due to the different distortion of the VSe_6 octahedra, we find d^3 and d^2 configurations for V_1 and V_2-ions, respectively. As a result, the d orbitals of V_1 are half occupied and fully polarized in the spin up channel with a total spin $S = 3/2$, while for V_2, the two d-electrons occupy the spin down channel with $S = 1$, consistent with the experimental analysis.

To estimate the relative energy scales of the spin chains, we have mapped the total energies of the above magnetic configurations into an effective 1D Heisenberg model:

$$H = E_0 - \sum_{i<j} J_{ij} \vec{S_i} \vec{S_j}$$

where E_0 is a sum of the nonmagnetic part, J_{ij} are the exchange interactions between spin S_i and S_j at sites i and j, respectively [35]. The positive (negative) J_{ij} represents FM (AFM)

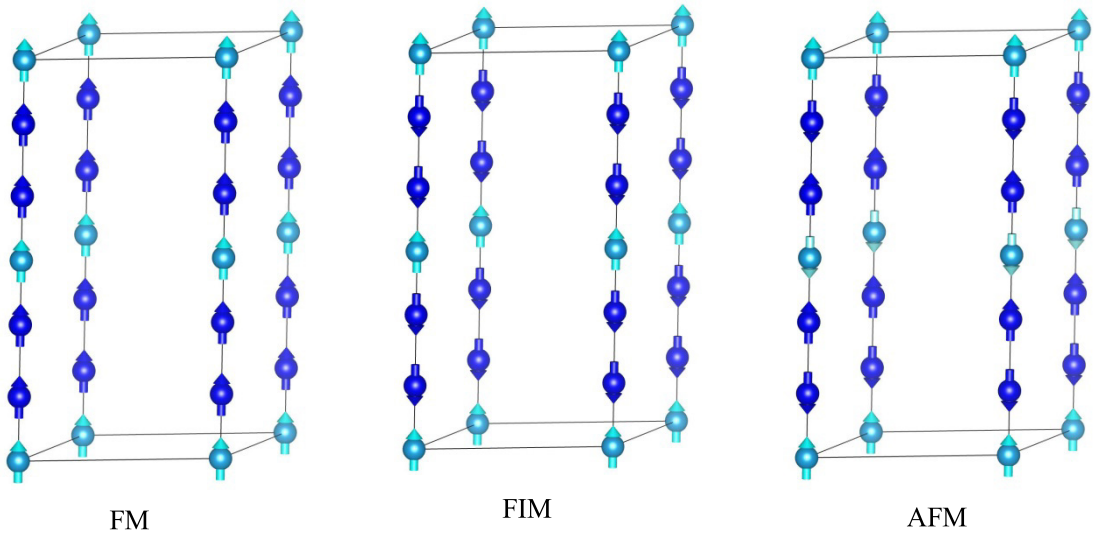

Figure 6. Different magnetic structures of $Ba_9V_3Se_{15}$.used in the numerical calculations.

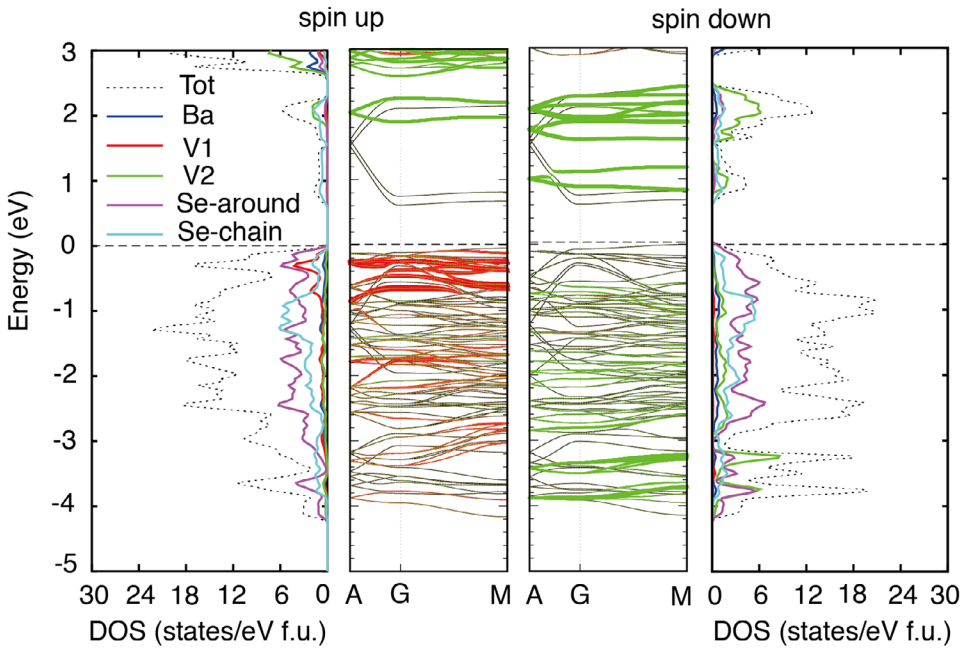

Figure 7. The DOS and band structures of $Ba_9V_3Se_{15}$ within GGA + U. Se-around denotes the Se-ions around the V-ions on the VSe_6 octahedron and Se-chain denotes other Se-ions forming quasi-1D chains.

coupling of the two spins. Here, we only give the intra-chain exchange couplings J_1 between the nearest neighboring V_1–V_2 and J_2 for V_2–V_2 (next nearest neighbors). The inter-chain exchange interactions are negligible because of the very long inter-chain distance. For one formula unit, the total energies associated with different magnetic order can be written as:

$$\begin{aligned} E\,(\mathrm{Fm}) &= E_0 - J_1 S_1 S_2 - J_2 S_2^2, \\ E\,(\mathrm{Afm}) &= E_0 + J_1 S_1 S_2 + J_2 S_2^2, \\ E\,(\mathrm{Fim}) &= E_0 + J_1 S_1 S_2 - J_2 S_2^2. \end{aligned} \tag{1}$$

Here, we use $S_1 = 3/2$ and $S_2 = 1$ for V_1 and V_2-ions, respectively. From the above equations, we obtain the magnetic interactions $J_1 = -676.28$ meV and $J_2 = 4.09$ meV, respectively. The resulting antiferromagnetic J_1 and ferromagnetic J_2 are in accordance with the ferrimagnetic ground state.

We note the above DFT analysis using decoupled 1D spin chains was only applied to estimate the intra-chain couplings. The real system contains three well-separated energy scales. While J_1 is responsible for the formation of the $V(2)^{(\downarrow)}V(1)^{(\uparrow)}$ $V(2)^{(\downarrow)}$ clusters, which takes place far above the experimental temperature range, J_2 governs the ferromagnetic spin chains and its magnitude is consistent with the experimental results. In addition, the magnetic interaction between neighboring spin chains is expected to be very small. However, as indicated in previous work [27], even a small inter-chain coupling could lead to a magnetic transition at finite temperature. This is consistent with our observation of the 3D magnetic transitions in $Ba_9V_3Se_{15}$. At very low temperatures, one may expect contributions from the 2D triangular lattice. However, above the transition, the system is governed by the spin wave excitations

of the ferromagnetic chains, as indicated by the $T^{1/2}$ contribution in the specific heat analysis. Detailed calculations based on above model may yield quantitative comparisons with experimental data, but this is beyond the scope of the current work. Nevertheless, our analysis of both the specific heat and susceptibility data seems to agree with the theoretical expectation of the ferromagnetic spin-1/2 chain in this temperature range.

Conclusion

In conclusion, the compound of $Ba_9V_3Se_{15}$ with spin chains has been synthesized under high-pressure and high-temperature conditions. It crystallizes into a hexagonal structure with the space group of *P*-6*c*2 (188). In the structure, the trimeric spin chains are along *c* axis and arranged in a triangular lattice in *ab*-plane. The distance of the adjacent spin chains is given by the lattice constant $a = 9.5745$ Å. $Ba_9V_3Se_{15}$ is a semiconductor with a band gap ~0.2 eV. It undergoes complex magnetic transitions. In the ZFC process with magnetic field of 10 Oe, $Ba_9V_3Se_{15}$ sequentially undergoes ferrimagnetic transition and spin cluster glass formation at 2.5 K and 3.3 K, respectively. A small magnetic field (>50 Oe) can eliminate the spin cluster glass state and the susceptibility merely presents ferrimagnetic transition. The specific heat at low temperature obtains a significant magnetic contribution that is proportional to $T^{1/2}$. $Ba_9V_3Se_{15}$ can be regarded as an effective ferromagnetic chains with effective spin-1/2 by the formation of $V(2)^{(\downarrow)}V(1)^{(\uparrow)}V(2)^{(\downarrow)}$ cluster. This might be a new route to bypass the large antiferromagnetic coupling and produce ferromagnetic spin chains in the experiment.

Acknowledgments

This work was financially supported by the National Science Foundation of China (NSFC) and the National Basic Research Program of China.

ORCID iDs

Xiancheng Wang https://orcid.org/0000-0001-6263-4963

References

[1] Gardner R A, Vlasse M and Wold A 1969 *Acta Crystallogr.* B **25** 781
[2] Imai H, Wada H and Shiga M 1996 *J. Phys. Soc. Japan* **65** 3460
[3] Nakamura H, Yamasaki T, Giri S, Imai H, Shiga M, Kojima K, Nishi M, Kakurai K and Metoki N 2000 *J. Phys. Soc. Japan* **69** 2763
[4] Inami T, Ohwada K, Kimura H, Watanabe M, Noda Y, Nakamura H, Yamasaki T, Shiga M, Ikeda N and Murakami Y 2002 *Phys. Rev.* B **66** 073108
[5] Fagot S, Foury-Leylekian P, Ravy S, Pouget J P and Berger H 2003 *Phys. Rev. Lett.* **90** 196401
[6] Lechermann F, Biermann S and Georges A 2005 *Phys. Rev. Lett.* **94** 166402
[7] Leininger P, Ilakovac V, Joly Y, Schierle E, Weschke E, Bunau O, Berger H, Pouget J P and Foury-Leylekian P 2011 *Phys. Rev. Lett.* **106** 167203
[8] Ilakovac V, Guarise M, Grioni M, Schmitt T, Zhou K, Braicovich L, Ghiringhelli G, Strocov V N and Berger H 2013 *J. Phys.: Condens. Matter* **25** 505602
[9] Forro L, Gaal R, Berger H, Fazekas P, Penc K, Kezsmarki I and Mihaly G 2000 *Phys. Rev. Lett.* **85** 1938
[10] Fagot S, Foury-Leylekian P, Ravy S, Pouget J P, Anne M, Popov G, Lobanov M V and Greenblatt W 2005 *Solid State Sci.* **7** 718
[11] Gauzzi A, Licci F, Barisic N, Calestani G L, Bolzoni F, Gilioli E, Marezio M, Sanna A, Franchini C and Forro L 2003 *Int. J. Mod. Phys.* B **17** 3503
[12] Kelber J, Reis A H, Aldred A T, Mueller M H, Massenet O, Depasquali G and Stucky G 1979 *J. Solid State Chem.* **30** 357
[13] Yamasaki T, Giri S, Nakamura H and Shiga M 2001 *J. Phys. Soc. Japan* **70** 1768
[14] Akrap A, Stevanovic V, Herak M, Miljak M, Barisic N, Berger H and Forro L 2008 *Phys. Rev.* B **78** 235111
[15] Herak M, Miljak M, Akrap A, Forro L and Berger H 2008 *J. Phys. Soc. Japan* **77** 093701
[16] Jenks J M, Hoggins J T, Rendon L E, Cohen S and Steinfink H 1978 *Inorg. Chem.* **17** 1773
[17] Zhang J *et al* 2017 *Inorg. Chem. Front.* **4** 1337
[18] Singh D J and Nordstrom L 2006 *Plane Waves, Pseudopotentials and the LAPW Method* 2nd edn (Berlin: Springer)
[19] Sjöstedt E, Nordström L and Singh D J 2000 *Solid State Commun.* **114** 15
[20] Blaha P, Schwarz K, Madsen G K H, Kvasnicka D and Luitz J 2014 *WIEN2K: an Augmented Plane Wave + Local Orbitals Program for Calculating Crystal Properties (Karlheinz Schwarz, Tech. Universitat Wien, Wien, Austria 2013)*
[21] Perdew J P, Burke K and Ernzerhof M 1996 *Phys. Rev. Lett.* **77** 3865
[22] Anisimov V I, Solovyev I V, Korotin M A, Czyzyk M T and Sawatzky G A 1993 *Phys. Rev.* B **48** 16929
[23] Assoud A, Soheilnia N and Kleinke H 2005 *J. Solid State Chem.* **178** 1087
[24] Assoud A, Soheilnia N and Kleinke H 2004 *Chem. Mater.* **16** 2215
[25] Souletie J, Rabu P and Drillon M 2005 *Phys. Rev.* B **72** 214427
[26] Mermin N D and Wagner H 1966 *Phys. Rev. Lett.* **17** 1133
[27] de Jongh L J and Miedema A R 2001 *Adv. Phys.* **50** 947
[28] Collins M F and Petrenko O A 1997 *Can. J. Phys.* **75** 605
[29] Fisher M E 1964 *Am. J. Phys.* **32** 343
[30] Bonner J C and Fisher M E 1964 *Phys. Rev.* **135** 640
[31] Xiang T 1998 *Phys. Rev.* B **58** 9142
[32] Kurniawan B, Ishikawa M, Kato T, Tanaka H, Takizawa K and Goto T 1999 *J. Phys.: Condens. Matter* **11** 9073
[33] Hardy V, Lambert S, Lees M R and Paul D M 2003 *Phys. Rev.* B **68** 014424
[34] Keller G, Held K, Eyert V, Vollhardt D and Anisimov V I 2004 *Phys. Rev.* B **70** 205116
[35] Anderson P W 1963 *Solid State Phys.* **14** 99